First- and Second-Generation Heterometallic Dendrimers Containing Ferrocenyl–Ruthenium(II)–Arene Motifs: Synthesis, Structure, Electrochemistry, and Preliminary Cell Proliferation...

ARTICLE *in* ORGANOMETALLICS · OCTOBER 2014

Impact Factor: 4.13 · DOI: 10.1021/om500809g

ORGANOMETALLICS

Article

pubs.acs.org/Organometallics

First- and Second-Generation Heterometallic Dendrimers Containing Ferrocenyl−Ruthenium(II)−Arene Motifs: Synthesis, Structure, Electrochemistry, and Preliminary Cell Proliferation Studies

Preshendren Govender,[†] Heidi Lemmerhirt,[‡] Alan T. Hutton,[†] Bruno Therrien,[§] Patrick J. Bednarski,[‡] and Gregory S. Smith*[,†]

[†]Department of Chemistry, University of Cape Town, Rondebosch 7701, Cape Town, South Africa

[‡]Department of Pharmaceutical and Medicinal Chemistry, Institute of Pharmacy, Ernst-Moritz-Arndt University Greifswald, 17487 Greifswald, Germany

[§]Institute of Chemistry, University of Neuchatel, 51 Ave de Bellevaux, CH-2000 Neuchatel, Switzerland

Supporting Information

ABSTRACT: Four first- and second-generation heterometallic ferrocenyl derived *p*-cymene-Ru(II) metallodendrimers, of general formula $[DAB\text{-}PPI\{(\eta^6\text{-}p\text{-cymene})Ru((C_7H_5NO)\text{-}\kappa^2\text{-}N,O)PTA(5\text{-ferrocenylvinyl})\}_n][PF_6]_n$ and $[DAB\text{-}PPI\{(\eta^6\text{-}p\text{-cymene})Ru((C_6H_5N_2)\text{-}\kappa^2\text{-}N,N)Cl(5\text{-ferrocenylvinyl})\}_n][PF_6]_n$ (where n = 4 ($\mathbf{G_1}$), 8 ($\mathbf{G_2}$), DAB = 1,4-diaminobutane, PPI = poly(propyleneimine), PTA = 1,3,5-triaza-7-phosphatricyclo[3.3.1.1]decane) have been synthesized. All complexes have been characterized using analytical (i.e., HR-ESI mass spectrometry, HPLC, elemental analysis, and cyclic voltammetry) and spectroscopic (i.e., ^1H and $^{13}C\{^1H\}$ NMR and infrared) methods. Electrochemical studies reveal that the *N,O*-*p*-cymene-Ru(II)-PTA complexes result in two irreversible redox processes (oxidation of the Fe(II) and Ru(II) centers), while the *N,N*-*p*-cymene-Ru(II) complexes display one reversible wave (Fe(II)/Fe(III) couple). Heterometallic model complexes have been prepared, and for one of the complexes, its molecular structure has been determined by single-crystal X-ray crystallography. *In vitro* antiproliferation activity of the dendritic ligands and their complexes were evaluated against A2780 and A2780cisR human ovarian cancer lines, the SISO human cervix cancer line, the LCLC-103H human lung cancer line, and the 5637 human bladder cancer line. Nine of the twelve compounds slowed the growth of the ovarian cancer cell lines by more than 50% at equi-iron concentrations of 5 μM.

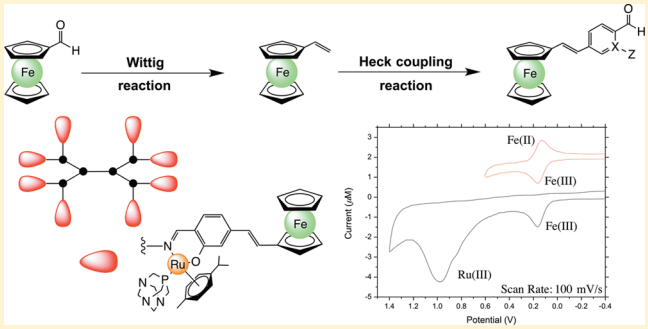

INTRODUCTION

After the discovery of platinum-based anticancer drugs,[1] ruthenium compounds were investigated as therapeutic agents, as the platinum-based drugs are poorly selective and produce several undesirable side effects.[2] Ruthenium is less toxic than platinum, with its biological activity attributed to its ability to mimic the behavior of iron and bind to biomolecules, such as human serum albumin and transferrin.[3] Two inorganic Ru(III) complexes, namely NAMI-A ($H_2Im[trans\text{-}RuCl_4(DMSO)(Him)]$ (Him = imidazole))[4] and KP1339 ($H_2Na[trans\text{-}RuCl_4(Hind)_2]$ (Hind = indazole)),[5] are currently progressing through clinical trials, with the former active against solid metastases, whereas KP1339 displays profound activity against neuroendocrine tumors (NET). The activity of the Ru(III) complexes is thought to be brought on by reduction *in vivo* to the more reactive Ru(II) species.[6] As a consequence, Ru(II) complexes of general formula $[(\eta^6\text{-arene})Ru(X)(Y)(Z)]$, where X and Y are bidentate chelating groups (*NN*, *NO*, *OO*, *SO*) or two monodentate ligands and Z is a monodentate moiety, often a leaving group, have been extensively studied as anticancer agents.[7] RAPTA compounds of general formula $[(\eta^6\text{-arene})Ru(PTA)Cl_2]$ (where PTA = 1,3,5-triaza-7-phosphatricyclo[3.3.1.1]decane) have been extensively studied,[8] although most are not particularly cytotoxic.[9] However, *in vivo* they display promising activity against solid metastatic tumors[10] and exert a strong antiangiogenic effect.[11]

Research into the introduction of a second metal in the design of heterobimetallic complexes as potential anticancer agents has flourished.[12] One such metal is iron and, more specifically, the iron-based organometallic complex ferrocene.[13] Ferrocene-based molecules have become very attractive in the field of medicinal chemistry,[14] with the activity of these complexes attributed to their favorable electronic properties and ease of functionalization.[15] Furthermore, simple derivatives of ferrocene display good activity *in vitro*, with inhibition of tumors observed *in vivo*.[16] In the pursuit for new tamoxifen-like drugs, Jaouen and co-workers[17] synthesized ferrocifens from 1-

Received: August 6, 2014
Published: September 17, 2014

   dx.doi.org/10.1021/om500809g | *Organometallics* 2014, 33, 5535−5545

Scheme 1. Synthesis of *N,O*- and *N,N*-Ferrocenyl-Derived Precursors 1 and 2

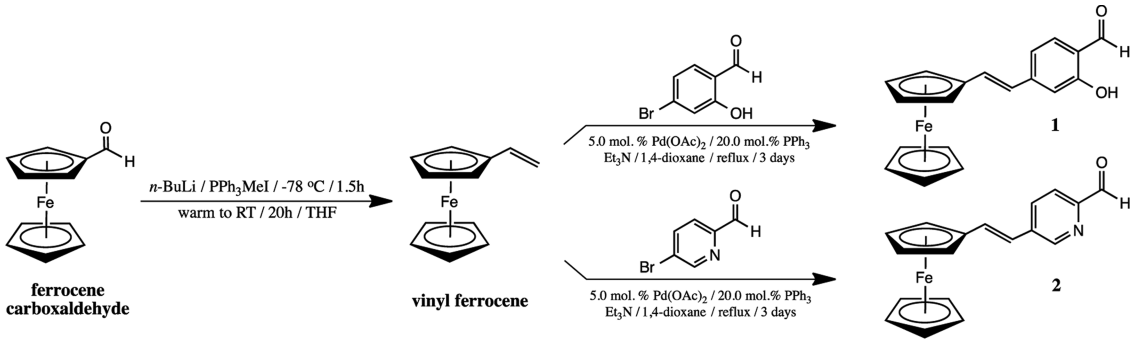

[4-(2-dimethylaminoethoxy)]-1-(phenyl-2-ferrocenylbut-1-ene), which are highly active ferrocenyl derivatives of the purely organic breast cancer drug tamoxifen. The increase in activity is attributed to the dual action of the organic drug and the Fenton chemistry (i.e., formation of singlet oxygen) of the Fe center.[18] Moreover, the stability of ferrocene in aqueous and aerobic media, the facility with which a large variety of derivatives may be prepared, and its favorable electrochemical properties have resulted in ferrocene becoming a promising molecule for incorporation in biological applications.[19]

In an effort to develop cytotoxic anticancer agents, ferrocene derivatives have been coupled with gold,[26] silver,[20] palladium,[12a] rhodium,[21] and iridium[21] complexes in order to achieve a synergistic effect between the two active metals. The introduction of the second metal resulted in cytotoxicities (in various cancer cell lines) comparable to that of the benchmark drug cisplatin. However, there are only a handful of reports where ruthenium and iron have been combined within the same molecule and investigated for anticancer activity.[22] The majority of these derivatives display moderate activity in comparison to cisplatin, while a heterobimetallic ruthenium hexamethylbenzene phosphinoferrocene amino derivative displays activity in the low micromolar range (~4 μM in A2780, human ovarian cancer cells),[22a] further providing motivation for this study.

Following the successes of cisplatin and the trinuclear Pt-based anticancer complex BBR3464,[23] researchers have used the polynuclear strategy by conjugating metallodrugs onto dendritic scaffolds in an effort to improve the overall biological activity.[24] Furthermore, the multivalency of dendrimers may lead to increased interactions between a dendrimer−drug conjugate and a target bearing multiple receptors. There are only a handful of metallodendrimers specifically developed to target cancerous cells.[25] We have reported the synthesis of a series of metallodendrimers containing half-sandwich organometallic ruthenium,[26] osmium,[27] iridium,[28] and rhodium[28] functionalities located on the periphery of a dendritic scaffold.

Herein, we report the synthesis of first- and second-generation heterometallic ferrocenyl-derived *N,O*-*p*-cymene-Ru(II)-PTA-salicylaldimine and *N,N*-*p*-cymene-Ru(II)-2-pyridylimine metallodendrimers ([**7**][PF_6]$_4$−[**10**][PF_6]$_8$). Furthermore, in order to compare size dependence on the biological activity, heterometallic model complexes ([**13**][PF_6] and [**14**][PF_6]) were synthesized as models for the larger metallodendrimers. The presence of heterometallic active sites contained in biological metalloenzymes has led us to explore the synthesis of heterometallic dendrimers by incorporating a ferrocenyl group into the *p*-cymene-ruthenium metallodendrimers previously reported by us,[26b,c] in an effort to improve the antitumor activity of these complexes.

RESULTS AND DISCUSSION

Synthesis of *N,O*- and *N,N*-Ferrocenyl-Derived Precursors. Synthesis of the ferrocenyl-derived precursors **1** and **2** required the preparation of vinylferrocene,[29] via a Wittig reaction, from ferrocenecarboxaldehyde. The ferrocenyl-derived precursors (4*E*)-(4-ferrocenylvinyl)-2-hydroxybenzaldehyde (**1**) and (5*E*)-(5-ferrocenylvinyl)-2-pyridinecarboxaldehyde (**2**) were prepared via a Heck coupling reaction of vinylferrocene and the appropriate aryl bromide (Scheme 1). The method described by Reyes et al.[30] was modified for the preparation of **1** and **2**. The Pd catalyst, triphenylphosphine, triethylamine, vinylferrocene, and the appropriate aldehyde were heated under reflux for 3 days in 1,4-dioxane, to afford **1** and **2** as purple solids in low yields (10−25%). **1** and **2** are soluble in most organic solvents such as dichloromethane, methanol, toluene, diethyl ether, and dimethyl sulfoxide.

The ^{1}H and ^{13}C{^{1}H} NMR spectra of **1** and **2** affirm the coupling of the two starting materials. The characteristic singlet for the presence of a highly deshielded proton on an aldehyde functionality is observed for both **1** (Figure S1, Supporting Information) and **2** (Figure S2, Supporting Information) at ~10 ppm. Three doublets of doublets (observed in the ^{1}H NMR spectrum of vinylferrocene) disappear, and two doublets (~6.7 and ~7.1 ppm) appear and are assigned to the two protons on the alkene moiety for both **1** and **2**, suggesting C−C bond formation. The two doublets have a coupling constant of $^3J_{HH} \approx 16$ Hz each, suggesting that the alkene moieties of **1** and **2** adopt a trans conformation rather than a cis conformation, as typical coupling constants for a cis conformation would be much lower ($^3J_{HH} \approx 9$ Hz).[31] A similar coupling constant (i.e., $^3J_{HH} = 16$ Hz) was reported by Yang et al., for the structurally similar compound (4*E*)-(4-ferrocenylvinyl)pyridne.[32] A strong sharp stretching vibration is observed in the infrared (IR) spectra at 1614 and 1575 cm^{-1} for **1** and **2**, respectively, and is assigned to the C=C bond of the alkene moiety. This observation further confirms successful C−C bond formation via the Heck reaction. The HR-ESI mass spectra of **1** and **2** give a base peak for [M + H]$^+$ ions at m/z 333.0562 and 318.0580, respectively, consistent with the proposed structures. Analytical HPLC traces were obtained for **1** and **2**, with single peaks observed at t_R = 17 and 16 min, respectively, attesting to the purity of these compounds.

Synthesis of Ferrocenyl-Derived Dendritic Ligands. The third step in the synthesis involved preparation of the two ferrocenyl-derived *N,O*-salicylaldiminato dendritic ligands **3** and

dx.doi.org/10.1021/om500809g | *Organometallics* 2014, 33, 5535−5545

Scheme 2. Synthesis of *N,O*- and *N,N*-Ferrocenyl-Derived Dendritic Ligands 3−6

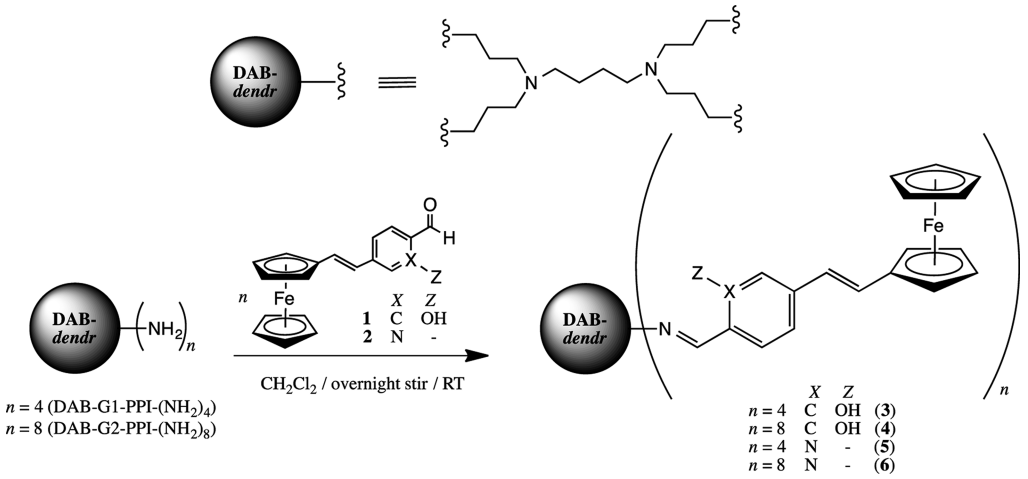

Scheme 3. Synthesis of Ferrocenyl-Derived Cationic *N,O*-*p*-cymene-Ru(II)-PTA and *N,N*-*p*-cymene-Ru(II) Metallodendrimers [7][PF_6]$_4$−[10][PF_6]$_8$

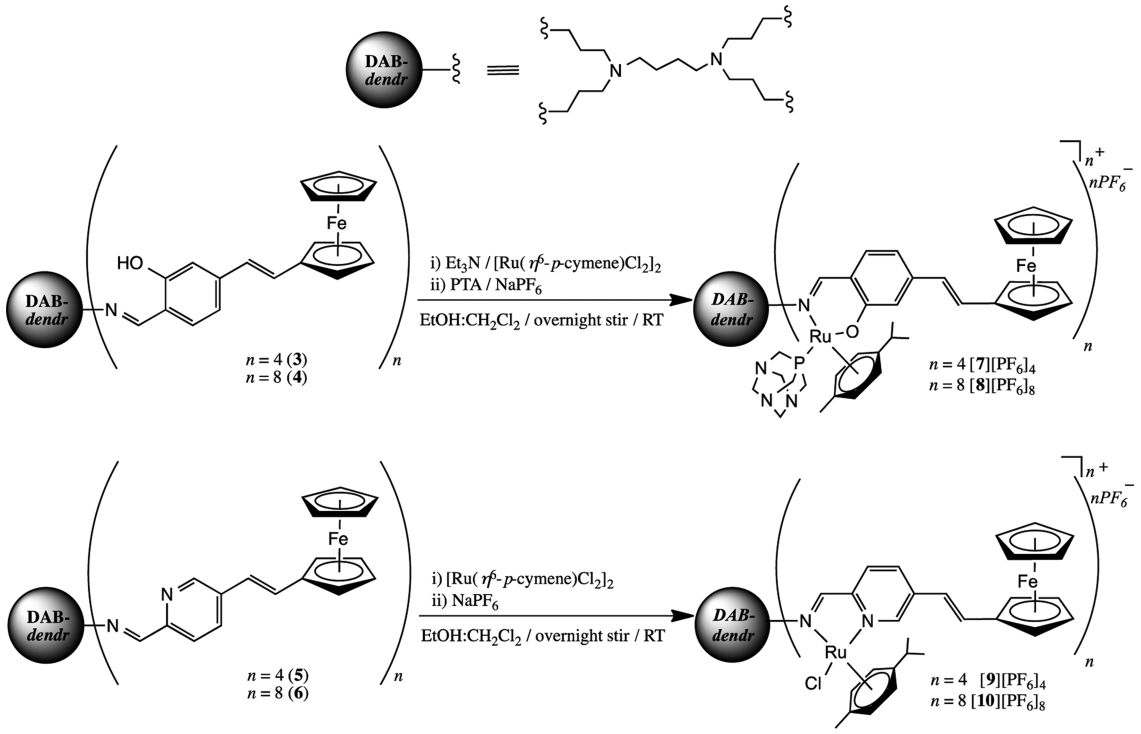

4 and the two ferrocenyl-derived *N,N*-pyridylimine dendritic ligands **5** and **6**. The dendritic ligands **3**−**6** were prepared via a Schiff base condensation of **1** (for **3** and **4**) or **2** (for **5** and **6**) with the amino groups of DAB-G_1-PPI-$(NH_2)_4$ (where DAB = 1,4-diaminobutane and PPI = poly(propyleneimine), for **3** and **5**) or of DAB-G_2-PPI-$(NH_2)_8$ (for **4** and **6**) in dichloromethane (Scheme 2). The dendritic ligands **3**−**6** were isolated as orange solids in moderate yields (50−65%). The dendritic ligands **3**−**6** are air and moisture stable, are soluble in a handful of solvents, such as dichloromethane, chloroform, acetonitrile, and dimethyl sulfoxide, and are insoluble in protic and nonpolar solvents.

The ^{1}H and ^{13}C{^{1}H} NMR data of **3**−**6** display overlapping and broadening of signals, similarly observed with other poly(propyleneimine) dendrimers functionalized at the periphery with inorganic and organic moieties.[26b,33] There is a disappearance of the singlet at ∼10 ppm (aldehyde proton of **1** and **2**) in the ^{1}H NMR spectrum of **3**−**6** (Figures S3−S6, Supporting Information), with an appearance of a broad singlet at ∼8.2 ppm (for **3** and **4**) and ∼8.4 ppm (for **5** and **6**), which is assigned to the proton of the newly formed imine bond. Typically, the signals for the aliphatic protons on the dendritic core and dendritic arms appear in the region between 1.4 and 3.7 ppm for **3**−**6**. The carbonyl carbon singlet observed in the ^{13}C{^{1}H} NMR spectrum of **1** and **2**, at ∼195 and ∼193 ppm, respectively, was not observed in the ^{13}C{^{1}H} NMR spectrum of **3**−**6**. This observation further confirms formation of the imine bond, as a singlet in the ^{13}C{^{1}H} NMR spectrum at ∼164 ppm (for **3** and **4**) and at ∼162 ppm (for **5** and **6**) is observed and is assigned to the carbon of the imine bond. The IR spectra of **3** and **4** display a strong broad stretching vibration

dx.doi.org/10.1021/om500809g | *Organometallics* 2014, 33, 5535−5545

Scheme 4. Synthesis of N,O- and N,N-Ferrocenyl-Derived Monomeric Ligands 11 and 12

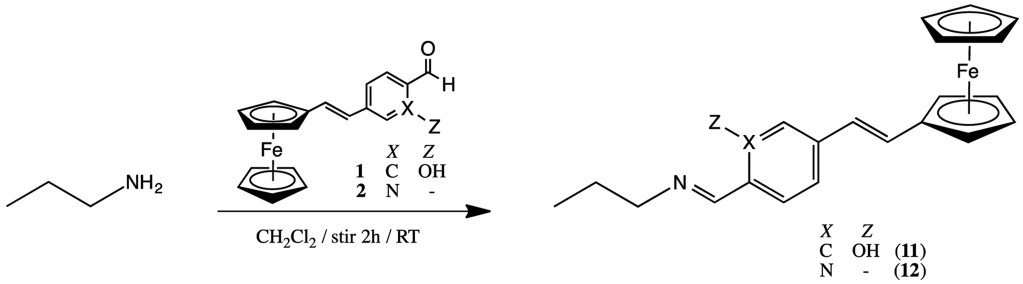

at ~1610 cm^{-1}, which is assigned to both the C═N and C═C bonds of the imine and alkene moieties, respectively. However, **5** and **6** display two bands of medium intensity, at ~1580 and ~1640 cm^{-1}, and these are assigned to the alkene and imine bonds, respectively. Following extensive drying of **3**–**6**, satisfactory elemental analysis data was not obtained, as the percentages obtained were outside acceptable limits and are ascribed to possible solvent inclusions. The inclusion of small molecules has been observed with purely organic dendrimers, as the free rotation of the dendritic arms allows for folding onto one another, in turn trapping small molecules.[33] Thus, the inclusion of dichloromethane resulted in C, H, and N percentages for **3**–**6** to fall within acceptable limits. HR-ESI mass spectrometry was used to confirm the proposed structures of **3**–**6**, with all complexes exhibiting a base peak corresponding to a charged complex.

Synthesis of Ferrocenyl-Derived Heterometallic Metallodendrimers. The metallodendrimers [**7**][PF_6]$_4$–[**10**][PF_6]$_8$ were synthesized by reacting the appropriate first- or second-generation dendritic ligand (**3**–**6**) with the ruthenium dimer [Ru(η^6-*p*-cymene)Cl_2]$_2$ in an ethanol/dichloromethane (50/50% v/v) mixture at room temperature (Scheme 3). The water-soluble PTA ligand was added to displace the chlorido ligand, in turn generating a cationic species. Metallodendrimers **7**–**10** were isolated as hexafluorophosphate salts, via a metathesis reaction with $NaPF_6$, to afford orange solids ([**7**][PF_6]$_4$ and [**8**][PF_6]$_8$) or dark purple solids ([**9**][PF_6]$_4$ and [**10**][PF_6]$_8$), in good yields (72–85%). Compounds [**7**][PF_6]$_4$–[**10**][PF_6]$_8$ are nonhygroscopic, air- and moisture-stable solids, can be stored over extended periods, and are soluble in dimethyl sulfoxide, acetone, and dimethylformamide and partially soluble in acetonitrile.

A comparison of the ^{1}H NMR spectra of [**7**][PF_6]$_4$–[**10**][PF_6]$_8$ to those of the corresponding dendritic ligands reveals chelation of the dendritic ligand to the ruthenium ion, which is confirmed by a slight downfield shift in the imine signal from ~8.0 ppm (for **3** and **4**) and ~8.3 ppm (for **5** and **6**) to ~8.1 ppm (for [**7**][PF_6]$_4$ (Figure S7, Supporting Information) and [**8**][PF_6]$_8$ (Figure S8, Supporting Information)) and ~8.9 ppm (for [**9**][PF_6]$_4$ (Figure S9, Supporting Information) and [**10**][PF_6]$_8$ (Figure S10, Supporting Information)) respectively. Coordination of the dendritic ligand to the ruthenium ion in [**7**][PF_6]$_4$–[**10**][PF_6]$_8$ results in a loss of 2-fold symmetry of the *p*-cymene moiety. This results in the methyl protons of the isopropyl group exhibiting two broad multiplets in the range 1.1–1.3 ppm (for [**7**][PF_6]$_4$–[**10**][PF_6]$_8$), with a broad multiplet observed at ~2.6 ppm assigned to the single proton on the isopropyl group.

The ^{1}H NMR spectra of [**7**][PF_6]$_4$ (Figure S7, Supporting Information) and [**8**][PF_6]$_8$ (Figure S8, Supporting Information) show signals in the range 5.5–7.2 ppm and are assigned to the aromatic protons. The signals for the protons on the PTA ligand (4.1–4.6 ppm) overlap with the broad signals assigned to the protons on the ferrocenyl functionality and the diastereotopic protons (as a result of the stereogenicity induced by the ruthenium ion) on the aliphatic carbon adjacent to the imine nitrogen. Furthermore, the signals for the PTA ligand display the typical splitting pattern for an AB spin system and correlate well with splitting patterns observed with other PTA complexes in the literature.[34] The ^{31}P{^{1}H} NMR spectra of [**7**][PF_6]$_4$ and [**8**][PF_6]$_8$ display a singlet at ~–32 ppm, suggesting a single phosphine species and further attesting to the purity of these complexes.

On the other hand, chirality induced by coordination to the ruthenium ion results in the appearance of two broad multiplets (4.4–4.8 ppm) in the ^{1}H NMR spectrum of metallodendrimers [**9**][PF_6]$_4$ (Figure S9, Supporting Information) and [**10**][PF_6]$_8$ (Figure S10, Supporting Information), which are assigned to the diastereotopic protons on the dendritic arms. These broad multiplets overlap with the two broad doublets assigned to the protons on the substituted ferrocenyl functionality, while the protons on the unsubstituted ferrocenyl functionality appear as a singlet at 4.2 ppm.

The ^{13}C{^{1}H} NMR data for metallodendrimers [**7**][PF_6]$_4$ and [**8**][PF_6]$_8$ display two singlets for the carbon atoms of the PTA ligand in the range 51–72 ppm, confirming coordination to the ruthenium ion and displacement of the chlorido ligand. Upon coordination of the ligand to the ruthenium ion, IR data of [**7**][PF_6]$_4$–[**10**][PF_6]$_8$ display a distinct shift in the C═C_{alkene} and C═N_{imine} stretching vibrations from ~1613 cm^{-1} (for **3** and **4**) to ~1590 cm^{-1} (for [**7**][PF_6]$_4$ and [**8**][PF_6]$_8$) and a similar shift to lower wavenumbers of the C═N_{imine} stretching vibration for metallodendrimers [**9**][PF_6]$_4$ and [**10**][PF_6]$_8$, from ~1640 cm^{-1} (for **5** and **6**) to ~1625 cm^{-1}, is observed. The inclusion of dichloromethane resulted in C, H, and N percentages for [**7**][PF_6]$_4$–[**10**][PF_6]$_8$ to fall within acceptable limits. In addition, HR-ESI mass spectrometry for the first-generation metallodendrimers [**7**][PF_6]$_4$ and [**9**][PF_6]$_4$ exhibit a base peak corresponding to 6+ and 5+ charged ions, respectively. However, the second-generation derivatives [**8**][PF_6]$_8$ and [**10**][PF_6]$_8$ depict a multicharged ion complex and a molecular ion peak in the mass spectrum, respectively.

Synthesis of Ferrocenyl-Derived Monomeric Ligands and Ferrocenyl-Derived Heterometallic Model Complexes. The monomeric ferrocenyl-derived ligands **11** and **12** were synthesized in a similar manner to their dendritic derivatives **3**–**6**, by reaction of *n*-propylamine with **1** and **2** (Scheme 4), via a Schiff base condensation reaction. Following purification over a small pad of silica, the new monomeric ligands **11** and **12** were isolated as orange-red solids in 56% and 71% yields, respectively.

dx.doi.org/10.1021/om500809g | *Organometallics* 2014, 33, 5535–5545

Scheme 5. Synthesis of Ferrocenyl-Derived Cationic *N,O*-Ru(II)-*p*-cymene-PTA and *N,N*-*p*-cymene-Ru(II) Heterometallic Model Complexes [13][PF_6] and [14][PF_6]

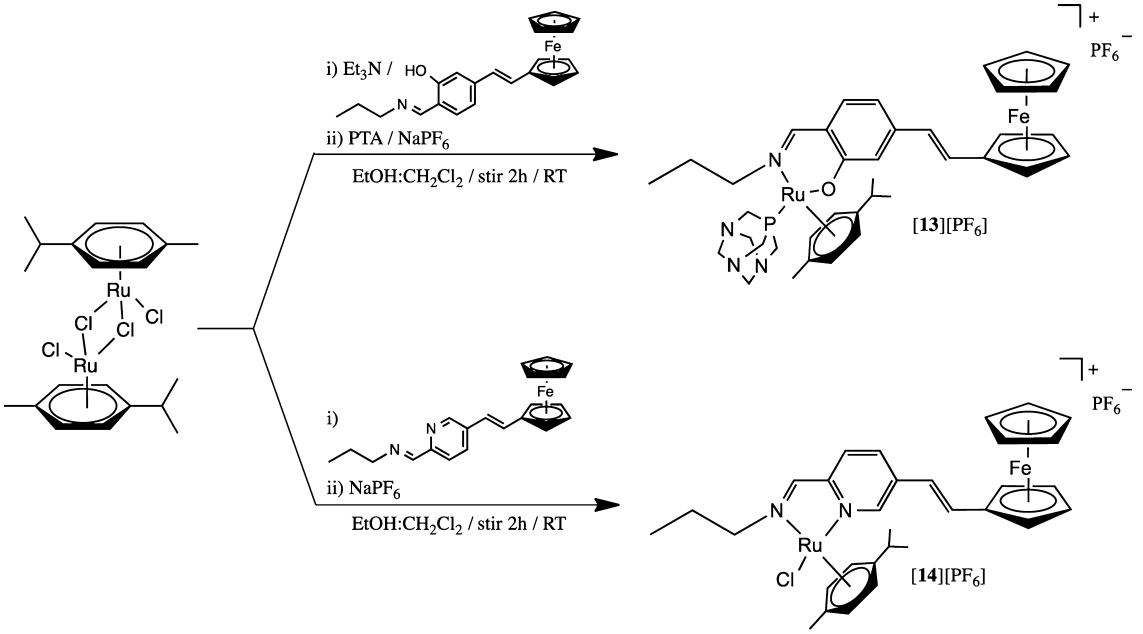

In order to compare size dependence on the biological activity, the heterometallic model complexes [**13**][PF_6] and [**14**][PF_6] of the ferrocenyl-derived ruthenium-*p*-cymene metallodendrimers were prepared. Two equivalents of the monomeric ligand **11** or **12** was reacted with 1 equiv of the ruthenium arene dimer [Ru(η^6-*p*-cymene)Cl_2]$_2$ by stirring at room temperature in ethanol/dichloromethane (50/50% v/v) (Scheme 5), in the presence of triethylamine (for the preparation of [**13**][PF_6]). PTA was added to the reaction mixture containing the *N,O*-salicylaldiminato ligand **11**, which displaced the chlorido ligand and generated a cationic complex. The new heterometallic model complexes [**13**][PF_6] and [**14**][PF_6] were isolated as orange and dark purple hexafluorophosphate salts, respectively, and have solubilities in polar solvents similar to those of their dendritic counterparts [**7**][PF_6]$_4$−[**10**][PF_6]$_8$. The synthesis and purity of the monomeric ligands **11** and **12** and heterometallic model complexes [**13**][PF_6] and [**14**][PF_6] were confirmed by spectroscopic (^{1}H (Figures S11− S14, Supporting Information) and $^{13}C\{^1H\}$ NMR and infrared spectroscopy) and analytical techniques (HPLC, elemental analysis, and mass spectrometry).

X-ray Crystallography. The trans conformation of the alkene moiety was also confirmed from a single-crystal X-ray structure analysis of **1** (Figure 1). In the solid state, the hydroxybenzaldehyde group was found to be coplanar with the cyclopentadienyl unit, thus suggesting an optimal electronic delocalization in **1** with a C5−C8−C9−C10 torsion angle of −179.1(2)°. Crystallographic details of **1** are summarized in Table S1 (Supporting Information).

The molecular structure of the mononuclear complex [**13**][PF_6] was also elucidated by a single-crystal X-ray diffraction analysis. Crystals were grown by slow evaporation of a solution of [**13**][PF_6] in acetone and crystallized in the monoclinic space group $P2_1/c$. An ORTEP drawing of [**13**][PF_6]·H_2O is shown in Figure 2, together with selected geometrical parameters. In [**13**]$^+$, the ferrocenyl unit adopts an eclipsed conformation and the trans conformation of the vinylic

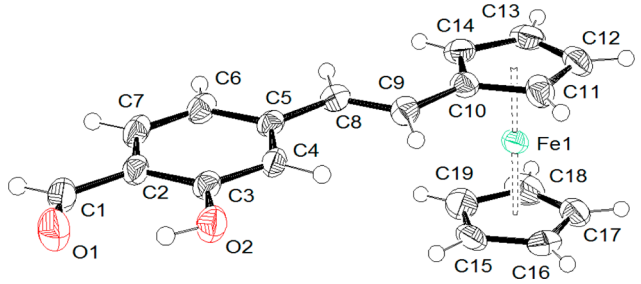

Figure 1. ORTEP representation of **1**, with thermal ellipsoids at the 50% probability level. Selected bond lengths (Å) and angles (deg): O1−C1 1.227(3), O2−C3 1.360(3), C8−C9 1.339(3); O1−C1−C2 124.5(3), O2−C3−C2 121.1(2), C5−C8−C9 126.3(2).

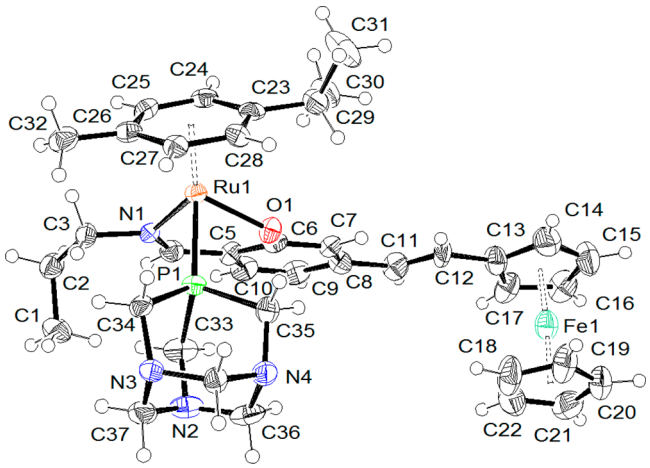

Figure 2. ORTEP representation of [**13**]$^+$, with thermal ellipsoids at the 50% probability level. The water molecule and the PF_6 anion have been omitted for clarity. Selected bond lengths (Å) and angles (deg): Ru1−N1 2.097(5), Ru1−O1 2.068(4), Ru1−P1 2.305(2), O1−C6 1.324(7), C11−C12 1.331(11); P1−Ru1−O1 80.5(1), P1−Ru1−N1 86.9(1), O1−Ru1−N1 87.5(2).

dx.doi.org/10.1021/om500809g | *Organometallics* 2014, 33, 5535−5545

Table 1. Redox Potentials (V vs Ag/Ag^+) of Metallodendrimers $[7][PF_6]_4$–$[10][PF_6]_8$, $[13][PF_6]$, $[14][PF_6]$, and ferrocene (Fc)[a]

	Fe(II)/Fe(III)						Ru(II)/Ru(III)
complex	E_{pa}	E_{pc}	ΔE_p[b]	$E_{1/2}$[c]	$\Delta E_{1/2}$[d]	i_{pa}/i_{pc}	E_{pa}
$[7][PF_6]_4$	0.16	n.o.					0.98
$[8][PF_6]_8$	0.17	n.o.					0.98
$[9][PF_6]_4$	0.23	0.15	0.08	0.19	0.07	1.14	n.o.
$[10][PF_6]_8$	0.22	0.15	0.07	0.19	0.07	1.46	n.o.
$[13][PF_6]$	0.18	n.o.					0.97
$[14][PF_6]$	0.23	0.16	0.07	0.20	0.08	0.98	n.o.
Fc	0.17	0.07	0.10	0.12	0	0.99	

[a]Measured in CH_3CN at a scan rate of 100 mV s^{-1} ($[7][PF_6]_4$, $[8][PF_6]_8$, and $[13][PF_6]$) or 50 mV s^{-1} ($[9][PF_6]_4$, $[10][PF_6]_8$, and $[14][PF_6]$) and referenced to Ag/Ag^+. n.o. = not observed. [b]$\Delta E_p = E_{pa} - E_{pc}$, where E_{pa} and E_{pc} are the anodic and cathodic peak potentials vs Ag/Ag^+, respectively. [c]$E_{1/2} = (E_{pa} + E_{pc})/2$. [d]$\Delta E_{1/2} = E_{1/2}$(Fc compound) $- E_{1/2}$(Fc).

carbon–carbon double bond is further confirmed, the C8–C11–C12–C13 torsion angle being 177.1(7)°. The ruthenium atom is coordinated to the nitrogen and the oxygen atoms of the Schiff base ligand as well as to the phosphorus atom of the PTA ligand and an η^6-*p*-cymene ligand, thus leading to a typical chiral-at-metal pseudotetrahedral or "piano-stool" complex. The crystallographic details of $[13][PF_6]\cdot H_2O$ are summarized in Table S1 (Supporting Information).

In $[13]^+$ the average distance between the ruthenium and carbon atoms of the η^6-*p*-cymene ring is 2.23 Å, comparable to those in structurally similar ruthenium-*p*-cymene complexes reported in the literature.[26b] The Ru–P distance in $[13]^+$ (2.305(2) Å) is comparable to that observed in analogous ruthenium-arene-PTA compounds.[35] In the crystal structure, the cyclopentadienyl group attached to the vinyl moiety (plane defined by C13–C17) and the phenol group (plane defined by C5–C10) are not coplanar; an angle of 15.5° is found between these two planes. The presence of water molecules in the crystal packing of $[13][PF_6]$ generates a series of hydrogen bonds. The water molecule interacts with the PF_6^- group (O···F distance 3.017(8) Å with an O–H···F angle of 151.7°) and a nitrogen atom of the PTA ligand (O···N distance 2.866(9) Å with an O–H···N angle of 154.3°).

Electrochemistry. The different σ-donating and π-accepting capacities of the dendritic ligands **3**–**6** influence the oxidation potentials of the Ru(II) centers upon complexation. Furthermore, these potentials provide insight into the fundamental character of the ligands in the complexes. Previous reports suggest that ligands which favor oxidation of the ferrocenyl moiety can produce reactive oxygen species, which have the ability to disrupt lipid membranes and in turn influence the antitumor activity of the complexes.[36] Hence, to investigate such possible correlations in the current systems and to provide further characterization of the complexes, the metallodendrimers $[7][PF_6]_4$–$[10][PF_6]_8$ and model complexes $[13][PF_6]$ and $[14][PF_6]$ were studied by cyclic voltammetry at a Pt-disk working electrode in acetonitrile, containing $[n\text{-}Bu_4N][ClO_4]$ as the background electrolyte, a platinum-wire auxiliary electrode, and a Ag/Ag^+ reference electrode. A comparison of the relevant electrochemical data is given in Table 1.

The free ferrocene standard exhibits a one-electron reversible wave with $E_{1/2}$ = 0.12 V for the Fc/Fc^+ couple relative to the Ag/Ag^+ reference electrode. First- and second-generation metallodendrimers display similar voltammetric behaviors in acetonitrile, and hence representative cyclic voltammograms are shown in Figures 3 and 4 for the first-generation *N,O-p*-cymene-ruthenium-PTA metallodendrimer $[7][PF_6]_4$ and *N,N-p*-cymene-ruthenium metallodendrimer $[9][PF_6]_4$, respectively.

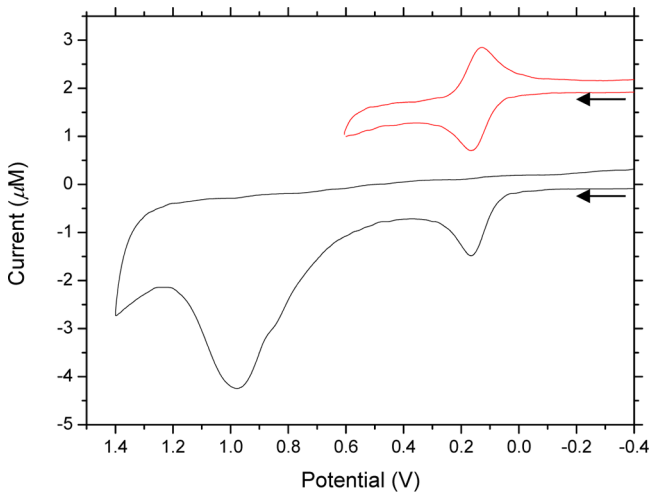

Figure 3. Cyclic voltammogram of $[7][PF_6]_4$ showing a partial (top) and a full scan (bottom), as recorded in acetonitrile (scan rate 100 mV s^{-1}). The potential scale is referenced to Ag/Ag^+ (see the Experimental Section). The scan started at −0.40 V.

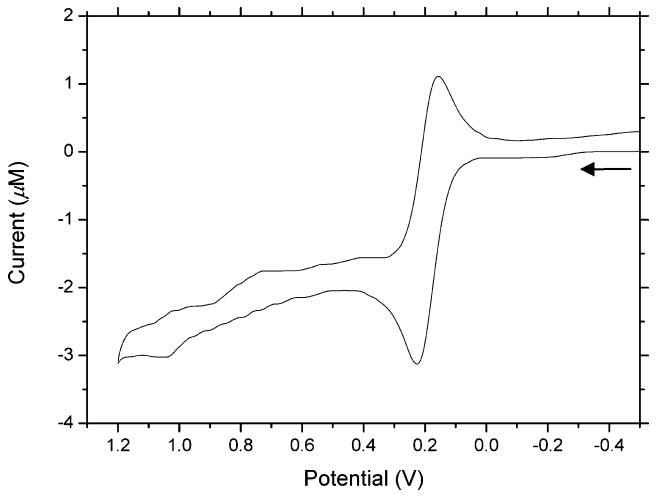

Figure 4. Cyclic voltammogram of $[9][PF_6]_4$ showing a full scan, as recorded in acetonitrile (scan rate 50 mV s^{-1}). The potential scale is referenced to Ag/Ag^+ (see the Experimental Section). The partial voltammogram is shifted by +2 μA to avoid overlap. The scan started at −0.50 V.

dx.doi.org/10.1021/om500809g | Organometallics 2014, 33, 5535–5545

Table 2. Relative Growth (in T/C_{corr} (%); See Eq 1) of Cells Treated with the Ferrocenyl-Derived Ligands and Their Heterometallic Complexes in Comparison to Untreated Controls[a]

			T/C_{corr} at 5 μM Fe (%)[b]				
compd	metal	n[c]	A2780[d]	A2780-cisR[d]	SISO[d]	LCLC-103H[d]	5637[d]
3	Fe	4	42.3 ± 34.2	37.3 ± 19.5	50.7 ± 18.3	66.5 ± 34.2	64.8 ± 20.0
4	Fe	8	21.1 ± 15.3	36.8 ± 21.7	37.2 ± 22.3	58.5 ± 28.7	19.8 ± 9.5
5	Fe	4	31.3 ± 28.4	29.4 ± 16.5	67.9 ± 18.6	75.8 ± 38.3	41.5 ± 15.4
6	Fe	8	23.0 ± 18.7	30.8 ± 21.5	71.8 ± 16.7	84.6 ± 37.7	41.6 ± 16.6
11	Fe	1	7.8 ± 10.1	18.6 ± 4.7	5.0 ± 4.4	31.9 ± 10.4	27.6 ± 8.2
12	Fe	1	26.0 ± 19.4	24.9 ± 20.6	64.8 ± 20.8	78.8 ± 38.3	38.1 ± 15.8
[**7**][PF_6]$_4$	Fe–Ru	8	−2.3 ± 5.6	−4.3 ± 1.5	73.0 ± 64.4	103.7 ± 10.1	57.6 ± 26.4
[**8**][PF_6]$_8$	Fe–Ru	16	5.5 ± 12.6	−1.8 ± 4.2	95.3 ± 61.9	103.1 ± 28.9	67.6 ± 33.8
[**9**][PF_6]$_4$	Fe–Ru	8	86.1 ± 26.3	59.9 ± 12.7	90.4 ± 13.9	42.5 ± 14.1	10.8 ± 13.4
[**10**][PF_6]$_8$	Fe–Ru	16	107.6 ± 97.8	42.5 ± 13.1	105.2 ± 51.4	40.7[e]	54.4[e]
[**13**][PF_6]	Fe–Ru	2	70.3 ± 16.0	54.6 ± 5.8	100.2 ± 5.4	102.5 ± 16.5	34.2 ± 20.5
[**14**][PF_6]	Fe–Ru	2	12.0 ± 9.6	25.5 ± 8.9	22.9 ± 11.6	84.2 ± 29.9	12.6 ± 10.9

[a]Compounds were tested against five human cancer cell lines after 96 h exposure to compound at 5 μM Fe, relative to untreated control. [b]Concentrations normalized to the mole equivalents of Fe in each complex. [c]n = Number of metals present in the complex. [d]Average of three or more independent experiments ± standard deviation. [e]Average of two determinations.

The redox potentials of [**7**][PF_6]$_4$ and [**8**][PF_6]$_8$ were measured at a scan rate of 100 mV s^{-1}, and ferrocene was used as the internal standard. Both [**7**][PF_6]$_4$ (Figure 3, bottom) and [**8**][PF_6]$_8$ (Figure S15, bottom (Supporting Information)) exhibit similar voltammograms with two irreversible oxidation waves in the positive region. The ferrocenyl oxidation wave (Fe(II) → Fe(III)) appears at E_{pa} = 0.16 and 0.17 V for [**7**][PF_6]$_4$ and [**8**][PF_6]$_8$, respectively. A second redox event for the oxidation of the ruthenium center (Ru(II) → Ru(III)) appears at 0.98 V for both [**7**][PF_6]$_4$ and [**8**][PF_6]$_8$ and is electrochemically irreversible, suggesting thermodynamic instability of the oxidation products.[37,38] On an oxidative scan with the switching potential set just after the first oxidation wave, a reversible one-electron ferrocene/ferrocenium redox wave is observed for both [**7**][PF_6]$_4$ (Figure 3, top) and [**8**][PF_6]$_8$ (Figure S15, top (Supporting Information)). Unlike other ruthenium–iron heterometallic systems,[22a,c,38a,39] where an irreversible wave for the ruthenium center and a reversible wave for the ferrocenyl moiety are common, here this is not observed. Instead, the oxidation of the Ru center inhibits the reversibility of the Fc/Fc^+ couple. However, the electrochemical studies performed on the reported heterometallic systems found in the literature were performed using different conditions (i.e., background electrolyte, reaction solvent, and/or the compound counterion), and these affect the redox processes compared. In the present study, the electrochemical data suggest that oxidation of the ruthenium center influences and prevents reduction of the ferrocenium species, resulting in the two irreversible redox processes observed for [**7**][PF_6]$_4$ and [**8**][PF_6]$_8$.

The redox potentials of [**9**][PF_6]$_4$ and [**10**][PF_6]$_8$ were measured at a scan rate of 50 mV s^{-1}. Due to the partial solubility of [**9**][PF_6]$_4$ and [**10**][PF_6]$_8$ in acetonitrile, a slower scan rate was chosen, as faster scan rates did not produce smooth cyclic voltammograms. The cyclic voltammograms for [**9**][PF_6]$_4$ (Figure 4) and [**10**][PF_6]$_8$ (Figure S16, Supporting Information) exhibit one reversible wave (current ratios (i_{pa}/i_{pc}) are close to unity) in the positive region and is assigned to the Fe(II)/Fe(III) couple.[22c,39c] However, there was no oxidation of Ru(II) observed and this is attributed to the electron-withdrawing nature of the chlorido ligand, which lowers the electron density at the ruthenium center, making the Ru oxidation more difficult. As expected, the ferrocene/ferrocenium redox potentials of [**9**][PF_6]$_4$ and [**10**][PF_6]$_8$ are nearly identical (Table 1). In comparison to free ferrocene ($E_{1/2}$ = 0.12 V), the ferrocenyl moiety of [**9**][PF_6]$_4$ and [**10**][PF_6]$_8$ is more difficult to oxidize ($E_{1/2}$ = 0.19 V), and this is attributed to the electron-withdrawing effects of the alkene moiety, the ruthenium center, and the overall positive charge of the complexes. This was similarly demonstrated for monosubstituted ferrocenyl-derived complexes containing electron-withdrawing groups bonded to the ferrocene ring.[40] As expected, both [**13**][PF_6] (Figure S17, Supporting Information) and [**14**][PF_6] (Figure S18, Supporting Information) exhibit similar cyclic voltammograms and wave potentials in comparison to their dendritic counterparts [**7**][PF_6]$_4$–[**10**][PF_6]$_8$.

Inhibition of Cancer Cell Proliferation. Preliminary *in vitro* cell proliferation studies of the ligands (**3**–**6**, **11**, and **12**) and their complexes ([**7**][PF_6]$_4$–[**10**][PF_6]$_8$, [**13**][PF_6], and [**14**][PF_6]) were evaluated against A2780 and A2780cisR human ovarian cancer lines, the SISO human cervix cancer line, the LCLC-103H human lung cancer line, and the 5637 human bladder cancer line (Table 2). We used a microtiter plate assay based on the staining of cells with crystal violet.[41] Cells were grown for 24 h following plating and then treated continuously for 96 h with the test compound. To express cell growth, the T/C_{corr} method was used (see eq 1 in the Experimental Section): a T/C_{corr} value of 100% indicates the same growth rate as the untreated controls over 96 h, a positive T/C_{corr} between 100 and 0% indicates slower cell growth relative to untreated controls, a T/C_{corr} value of 0 indicates no cell growth over 96, and a negative T/C_{corr} value indicates cytotoxicity, i.e., fewer cells after 96 h than at the time of treatment.

The cell proliferation studies of the ferrocenyl-derived compounds were initially performed at an equi-iron concentration of 20 and 10 μM; however, many of the compounds displayed very potent antiproliferative activity, and so no structure–activity relationships were observed. After the iron concentration for all compounds was lowered to 5 μM, both the ferrocenyl-derived ligands (**3**–**6**, **11**, and **12**) and ferrocenyl-derived *p*-cymene-ruthenium complexes ([**7**][PF_6]$_4$, [**8**][PF_6]$_8$, and [**14**][PF_6]) slowed the growth of both the A2780 and A2780cisR cell lines by more than 50% (Figure S19,

dx.doi.org/10.1021/om500809g | *Organometallics* 2014, 33, 5535–5545

Supporting Information), with the A2780 cell line being the most sensitive and showing no cross resistance to cisplatin. On the other hand, metallodendrimers [**9**][PF_6]$_4$ and [**10**][PF_6]$_8$ and complex [**13**][PF_6] were generally unable to inhibit cell growth of the ovarian lines by more than 50% at a 5 μM iron concentration (Table 2). The 5637 bladder cancer line was also quite sensitive to the antiproliferative effects of the tested compounds, while both the SISO and LCLC-103H lines were generally more resistant. Thus, the compounds possess a degree of selectivity for certain cancer cell lines, with a particularly strong activity in ovarian cancer. This selectivity should be characterized further in more ovarian cancer cell lines.

The relatively large error bars obtained for some of the ferrocenyl-derived complexes were attributed to the poor water solubility of the compounds in the culture medium, with precipitation sometimes observed at higher concentrations. Nevertheless, the ferrocenyl-derived *N,O* and *N,N* ligands (**3**−**6** and **12**) display moderate activity in all cell lines, with the monomeric ferrocenyl-derived *N,O*-salicylaldiminato ligand **11** displaying good activity (Figure S19, Supporting Information). However, there is no correlation between the size of the dendritic ligand and the activity observed. More specifically, it seems that the first- and second-generation ferrocenyl-derived *N,O*-*p*-cymene-ruthenium-PTA metallodendrimers [**7**][PF_6]$_4$ and [**8**][PF_6]$_8$ are the most active of the heterometallic series (Figure S19). There is an increase in activity observed when moving from the heterometallic model complex [**13**][PF_6] to the higher generation dendritic derivatives [**7**][PF_6]$_4$ and [**8**][PF_6]$_8$. Furthermore, introduction of the ruthenium-arene moiety does improve the activity in at least two of the metallodendrimers ([**7**][PF_6]$_4$ and [**8**][PF_6]$_8$) and may be attributed to possible transmembrane interactions and increased bioavailability brought on by the ferrocene moiety, similarly observed with ferrocifens.[17a,19,42] A similar trend was observed by Auzias et al., where ferrocenyl-derived ruthenium-arene complexes displayed improved *in vitro* antitumor activity against A2780 human ovarian cancer cells in comparison to their ferrocenyl-derived ligands.[22b] However, the improvement in activity is not observed for the ferrocenyl-derived *N,N*-*p*-cymene-ruthenium metallodendrimers [**9**][PF_6]$_4$ and [**10**][PF_6]$_8$ (Figure S19). It cannot be ruled out that the quite different redox potential of the ruthenium unit in [**7**][PF_6]$_4$ and [**8**][PF_6]$_8$ relative to [**9**][PF_6]$_4$ and [**10**][PF_6]$_8$ is responsible, at least in part, for the decrease in cytotoxicity. However, one of the next steps in the biological evaluation of the heterometallic ferrocenyl-derived ruthenium-arene metallodendrimers is to determine the IC_{50} values of the most active compounds. Hence, a direct comparison cannot be made between these heterometallic ferrocenyl-derived ruthenium-arene metallodendrimers mentioned and the homometallic ruthenium-arene metallodendrimers reported;[26b,c] these experiments are ongoing.

CONCLUSION

Heterometallic *N,O*- and *N,N*-ferrocenyl-derived ruthenium-arene metallodendrimers have been successfully synthesized. All complexes were characterized using an array of spectroscopic and analytical techniques, which confirmed formation of the desired compounds. Their heterometallic model complexes were prepared and characterized. Electrochemical studies were performed, revealing that the *N,O*-*p*-cymene-Ru(II)-PTA complexes result in two irreversible redox processes (oxidation of the Fe(II) and Ru(II) centers), while the *N,N*-Ru(II)-arene complexes display one reversible wave (Fe(II)/Fe(III) couple) in the positive region. Single-crystal X-ray diffraction was utilized to further confirm the proposed structures and illustrate the mode of coordination, through *N,O*- and *N,N*-donor atoms. Preliminary biological studies performed on the ferrocenyl-derived ligands and ferrocenyl-derived *p*-cymene-ruthenium complexes indicate that 9 of 12 compounds at equi-iron concentrations of 5 μM slowed the growth of both the A2780 and A2780cisR human cancer cell lines by more than 50% (i.e., IC_{50} < 5 μM). The complexes displayed no cross resistance to cisplatin. In three additional human cancer cell lines the activity was mostly reduced relative to that for the ovarian cancer lines. The first- and second-generation ferrocenyl-derived *N,O*-*p*-cymene-ruthenium-PTA metallodendrimers are the most active of the series.

EXPERIMENTAL SECTION

General Procedures. All reactions were performed under an inert atmosphere using a dual vacuum/nitrogen line and standard Schlenk-line techniques unless stated otherwise. All reaction solvents were dried by heating under reflux and under an inert atmosphere, over the appropriate drying agent, and all samples were dried under vacuum. 4-Bromo-2-hydroxybenzaldehyde, 5-bromo-2-pyridinecarboxaldehyde, triphenylphosphine, palladium acetate, triethylamine, DAB-G_1-PPI-$(NH_2)_4$, sodium hexafluorophosphate, and *n*-propylamine were purchased from Sigma-Aldrich; DAB-G_2-PPI-$(NH_2)_8$ was purchased from SyMO-Chem and used without further purification. Ruthenium(III) trichloride trihydrate was obtained as a generous donation from Johnson Matthey/Anglo-American Platinum Limited. Deuterated solvents were purchased from Sigma-Aldrich. Vinylferrocene[43a] and [Ru(η^6-*p*-cymene)Cl_2]$_2$[43b] were prepared according to literature procedures. Infrared (IR) spectra were measured as pure solids on a PerkinElmer Spectrum 100 FT-IR spectrometer equipped with a SMART iTR ATR unit. Intensity of stretching vibrations are marked as strong (s), medium (m), and weak (w). Melting points (mps) were determined using a Büchi B-540 instrument. Nuclear magnetic resonance (NMR) spectra were recorded on a Varian Unity XR400 spectrometer (^{1}H, 399.95 MHz; ^{13}C{^{1}H}: 100.58 MHz; ^{31}P{^{1}H}: 161.90 MHz) or Varian Mercury XR300 spectrometer (^{1}H: 300.08 MHz; ^{13}C{^{1}H}, 75.46 MHz; ^{31}P{^{1}H}, 121.47 MHz) or Bruker Biospin GmbH spectrometer (^{1}H, 400.22 MHz; ^{13}C{^{1}H}, 100.65 MHz; ^{31}P{^{1}H}, 162.00 MHz) at ambient temperature. Chemical shifts δ in ppm indicate a downfield shift relative to tetramethylsilane (TMS) and were referenced relative to the signal of the solvent.[44] Coupling constants *J* are given in Hz. Individual peaks are marked as singlet (s), doublet (d), doublet of doublets (dd), triplet (t), or multiplet (m). High-resolution electrospray ionization-mass spectrometry (HR-ESI-MS) was carried out on a Waters Synapt mass spectrometer. Data were recorded in positive ion mode. HPLC analysis was performed on a Dionex Ultimate 3000 instrument equipped with a ReproSil 100 column (C_{18} 5 μm, 4.6 or 10 mm diameter, 250 mm length) using a linear gradient of 5−90% MeOH/H_2O containing 0.1% TFA as the eluent over 40 min at a flow rate of 0.6 mL min^{-1} for analytical chromatography, respectively. Elemental analysis (C, H, N) was carried out using a Thermo Flash 1112 Series CHNS-O Analyzer. For certain metallodendrimers, the analyses are outside acceptable limits and are ascribed to the encapsulation of solvent molecules and/or other inorganic salts by the dendritic compounds. The preparation of compounds **1**−**6** and **11**−**14** is given in the Supporting Information.

Synthesis of Ferrocenyl-Derived Cationic *N,O*-*p*-cymene-Ru(II)-PTA Metallodendrimers [7][PF_6]$_4$ and [8][PF_6]$_8$. Triethylamine (0.017 mL, 0.122 mmol for [**7**][PF_6]$_4$; 0.039 mL, 0.279 mmol for [**8**][PF_6]$_8$) was added dropwise to a stirred solution of **3** (0.473 g, 0.0301 mmol for [**7**][PF_6]$_4$) or **4** (0.114 g, 0.0347 mmol for [**8**][PF_6]$_8$) in a EtOH/DCM (50/50, 60 mL) solution. The resulting orange solution was stirred at room temperature for 0.5 h. Next, [Ru(η^6-*p*-cymene)Cl_2]$_2$ (0.0377 g, 0.0616 mmol for [**7**][PF_6]$_4$; 0.0860 g, 0.140 mmol for [**8**][PF_6]$_8$) was added to the reaction mixture. The

dx.doi.org/10.1021/om500809g | *Organometallics* 2014, 33, 5535−5545

reaction mixture was stirred overnight at room temperature, and then the reaction mixture was filtered and PTA (0.0191 g, 0.122 mmol for [7][PF_6]$_4$; 0.0438 g, 0.279 mmol for [8][PF_6]$_8$) was added to the filtrate. The solution was stirred at room temperature for 6 h and filtered. A solution of $NaPF_6$ (0.0205 g, 0.122 mmol for [7][PF_6]$_4$; 0.0495 g, 0.279 mmol for [8][PF_6]$_8$) in EtOH (5 mL) was added to the filtrate at 0 °C and stirred for 1 h. The DCM was removed from the reaction mixture under reduced pressure, which resulted in the precipitation of an orange solid. The solid was isolated by filtration, washed with cold EtOH followed by Et_2O, and dried in vacuo.

*[DAB-**G**$_1$-PPI-{(η^6-p-cymene)Ru((C_7H_5NO)-κ^2N,O)PTA(5-ferrocenylvinyl)}$_4$][PF_6]$_4$ ([**7**][PF_6]$_4$).* Orange solid. Yield: 0.0807 g, 72.2%. IR (ATR): ν (cm^{-1}) 1590 (br s, alkene, C=C and imine, C=N). ^{1}H NMR ($(CD_3)_2CO$): δ (ppm) 1.13 and 1.27 (br m, 24H, $CH(CH_3)_{2\ p\text{-}cymene}$), 1.66 (br m, 4H, $NCH_2CH_{2\ core}$), 2.00 (m, 8H, $NCH_2CH_2CH_2N_{branch}$), 2.09 (br s, 12H, $CH_{3\ p\text{-}cymene}$), 2.16−2.26 (overlapping m, 12H, $NCH_2CH_{2\ core}$, $NCH_2CH_2CH_2N_{branch}$), 2.63 (br m, 4H, $CH(CH_3)_{2\ p\text{-}cymene}$), 3.96 (br m, 8H, $NCH_2CH_2CH_2N_{branch}$), 4.13 (br s, 20H, Cp-$CH_{unsubst\ ring}$), 4.22−4.55 (overlapping m, 64H, PTA, 2 × Cp-CH), 5.58 (br d, 4H, $Ar_{p\text{-}cymene}$), 5.83 (br d, 4H, $Ar_{p\text{-}cymene}$), 6.24 (br d, 4H, $Ar_{p\text{-}cymene}$), 6.40 (br d, 4H, $Ar_{p\text{-}cymene}$), 6.66 (d, ^3J = 16.2 Hz_{trans}, 4H, CH_{alkene}), 6.78 (br d, 4H, Ar), 6.85 (br s, 4H, Ar), 7.07 (d, ^3J = 16.0 Hz_{trans}, 4H, CH_{alkene}), 7.17 (m, 4H, Ar), 8.08 (br s, 4H, CH_{imine}). $^{13}C\{^1H\}$ NMR ($(CD_3)_2CO$): δ (ppm) 17.9, 20.9, 21.5 ($CH_{3\ p\text{-}cymene}$); 25.0, 53.9, 65.5, 68.3 (CH_2); 51.1, 51.2, 72.4, 72.5 ($CH_{2\ PTA}$); 67.1, 67.3, 69.4 (Cp-CH); 69.1 (Cp-$CH_{unsubst\ ring}$); 83.2 (C_{Cp}); 30.7, 82.9, 87.5, 88.8, 91.7 ($CH_{p\text{-}cymene}$); 97.5, 119.9 ($C_{p\text{-}cymene}$); 112.9, 119.3, 135.4 (CH_{Ar}); 118.5, 145.0, 164.5 (C_{Ar}); 125.4, 130.4 (CH_{alkene}); 165.6 (CH_{imine}). $^{31}P\{^1H\}$ NMR ($(CD_3)_2CO$): δ (ppm) −32.7 (s, PTA), −144.1 (sep, ^1J = 709.7 Hz, PF_6). Anal. Found for $C_{156}H_{196}N_{18}F_{24}Fe_4O_4P_8Ru_4$·3DCM (3973.589): C, 48.27; H, 5.76; N, 6.44. Calcd: C, 48.06; H, 5.12; N, 6.35. MS (HR-ESI-TOF, m/z): 627.7885 $[M + 2H]^{6+}$ (where M = [7][PF_6]$_4$ − 4PF_6). Mp: 166 °C (decomposes without melting).

*[DAB-**G**$_2$-PPI-{(η^6-p-cymene)Ru((C_7H_5NO)-κ^2N,O)PTA(5-ferrocenylvinyl)}$_8$][PF_6]$_8$ ([**8**][PF_6]$_8$).* Orange solid. Yield: 0.2013 g, 76.6%. IR (ATR): ν (cm^{-1}) 1590 (br s, alkene, C=C and imine, C=N). ^{1}H NMR ($(CD_3)_2CO$): δ (ppm) 1.12 and 1.26 (br d, 48H, $CH(CH_3)_{2\ p\text{-}cymene}$), 1.81−3.25 (overlapping m, 64H, $NCH_2CH_{2\ core}$, $NCH_2CH_{2\ core}$, $NCH_2CH_2CH_2N_{first\ branch}$, $NCH_2CH_2CH_2N_{first\ branch}$, $NCH_2CH_2CH_2N_{first\ branch}$, $NCH_2CH_2CH_2N_{second\ branch}$, $NCH_2CH_2CH_2N_{second\ branch}$), 2.20 (s, 24H, $CH_{3\ p\text{-}cymene}$), 2.60 (br m, 8H, $CH(CH_3)_{2\ p\text{-}cymene}$), 3.89 and 4.00 (br m, 16H, $NCH_2CH_2CH_2N_{second\ branch}$), 4.13 (br s, 40H, Cp-$CH_{unsubst\ ring}$), 4.13−4.61 (overlapping m, 128H, PTA, 2 × Cp-CH), 5.52 (m, 8H, $Ar_{p\text{-}cymene}$), 5.82 (m, 8H, $Ar_{p\text{-}cymene}$), 6.19 (m, 8H, $Ar_{p\text{-}cymene}$), 6.38 (m, 8H, $Ar_{p\text{-}cymene}$), 6.65 (br d, 8H, CH_{alkene}), 6.71 (m, 8H, Ar), 6.84 (br s, 8H, Ar), 7.05 (br d, 8H, CH_{alkene}), 7.22 (m, 8H, Ar), 8.13 (br s, 8H, CH_{imine}). $^{13}C\{^1H\}$ NMR ($(CD_3)_2CO$): δ (ppm) 18.0, 21.0, 21.4 ($CH_{3\ p\text{-}cymene}$); 23.5, 43.2, 59.2, 68.2 (CH_2); 51.1, 51.2, 72.5 ($CH_{2\ PTA}$); 67.1, 67.4, 69.5 (Cp-CH); 69.2 (Cp-$CH_{unsubst\ ring}$); 83.0 (C_{Cp}); 30.7, 82.9, 87.6, 88.8, 91.8 ($CH_{p\text{-}cymene}$); 97.2, 120.0 ($C_{p\text{-}cymene}$); 112.9, 119.2, 135.5 (CH_{Ar}); 118.6, 145.0, 164.5 (C_{Ar}); 125.5, 130.4 (CH_{alkene}); 165.7 (CH_{imine}). $^{31}P\{^1H\}$ NMR ($(CD_3)_2CO$): δ (ppm) −31.5 (s, PTA), −144.0 (sep, ^1J = 711.5 Hz, PF_6). Anal. Found for $C_{320}H_{414}N_{38}F_{48}Fe_8O_8P_{16}Ru_8$·9DCM (8348.252): C, 47.29; H, 6.60; N, 6.46. Calcd: C, 47.33; H, 5.22; N, 6.38. MS (HR-ESI-TOF, m/z): 247.1670 $[M + 18H]^{26+}$ (where M = [8][PF_6]$_8$ − 8PF_6). Mp: 285 °C (decomposes without melting).

Synthesis of Ferrocenyl-Derived Cationic *N,N*-*p*-cymene-Ru(II) Metallodendrimers [9][PF_6]$_4$ and [10][PF_6]$_8$. [Ru(η^6-*p*-cymene)Cl_2]$_2$ (0.0906 g, 0.148 mmol for [9][PF_6]$_4$; 0.0516 g, 0.0843 mmol for [10][PF_6]$_8$) was added to a stirred orange-red solution of **5** (0.0553 g, 0.0365 mmol for [9][PF_6]$_4$) or **6** (0.0659 g, 0.0208 mmol for [10][PF_6]$_8$) in a EtOH/DCM (50/50, 60 mL) solution. The dark purple reaction mixture was stirred overnight at room temperature, and then the reaction mixture was filtered. A solution of $NaPF_6$ (0.0249 g, 0.148 mmol for [9][PF_6]$_4$; 0.0281 g, 0.168 mmol for [10][PF_6]$_8$) in EtOH (5 mL) was added to the filtrate at 0 °C and stirred for 1 h. The DCM was removed from the reaction mixture under reduced pressure, which resulted in the precipitation of a dark purple solid. The solid was isolated by filtration, washed with cold EtOH followed by Et_2O, and dried in vacuo.

*[DAB-**G**$_1$-PPI-{(η^6-p-cymene)Ru(($C_6H_5N_2$)-κ^2N,N)Cl(5-ferrocenylvinyl)}$_4$][PF_6]$_4$ ([**9**][PF_6]$_4$).* Dark-purple solid. Yield: 0.0983 g, 84.7%. IR (ATR): ν (cm^{-1}) 1586 (s, alkene, C=C), 1623 (s, pyridyl and imine, C=N). ^{1}H NMR ($(CD_3)_2CO$): δ (ppm) 1.09 (br m, 24H, $CH(CH_3)_{2\ p\text{-}cymene}$), 1.30 (br m, 4H, $NCH_2CH_{2\ core}$), 2.00 (br m, 8H, $NCH_2CH_2CH_2N_{branch}$), 2.24 (br m, 4H, $NCH_2CH_{2\ core}$), 2.32 (br d, 12H, $CH_{3\ p\text{-}cymene}$), 2.62 (br m, 4H, $CH(CH_3)_{2\ p\text{-}cymene}$), 3.26 (br m, 8H, $NCH_2CH_2CH_2N_{branch}$), 4.19 (s, 20H, Cp-$CH_{unsubst\ ring}$), 4.43−4.78 (overlapping m, 24H, $NCH_2CH_2CH_2N_{branch}$, 2 × Cp-CH), 6.00 and 6.30 (m, 16H, $Ar_{p\text{-}cymene}$), 6.97 and 7.56 (m, 8H, CH_{alkene}), 8.10 (m, 4H, Pyr), 8.39 (m, 4H, Pyr), 8.88 (br s, 4H, CH_{imine}), 9.52 (br s, 4H, Pyr). $^{13}C\{^1H\}$ NMR ($(CD_3)_2CO$): δ (ppm) 18.6, 21.5, 22.0 ($CH_{3\ p\text{-}cymene}$); 24.5, 25.0, 51.2, 51.8, 52.7, 64.1 (CH_2); 68.0, 69.1, 70.6 (Cp-CH); 69.5 (Cp-$CH_{unsubst\ ring}$); 81.4 (C_{Cp}); 31.1, 83.9, 85.2, 85.6, 87.5 ($CH_{p\text{-}cymene}$); 104.9, 105.3 ($C_{p\text{-}cymene}$); 119.1, 137.3 (CH_{alkene}); 129.1, 133.4, 153.7 (CH_{Pyr}); 139.3, 151.5 (C_{Pyr}); 168.1 (CH_{imine}). Anal. Found for $C_{128}H_{148}N_{10}Cl_4F_{24}Fe_4P_4Ru_4$·4.5DCM (3558.1648): C, 44.45; H, 4.68; N, 3.84. Calcd: C, 44.73; H, 4.45; N, 3.94. MS (HR-ESI-TOF, m/z): 649.1115 $[M + H]^{5+}$ (where M = [9][PF_6]$_4$ − 4PF_6). Mp: 236 °C (decomposes without melting).

*[DAB-**G**$_2$-PPI-{(η^6-p-cymene)Ru(($C_6H_5N_2$)-κ^2N,N)Cl(5-ferrocenylvinyl)}$_8$][PF_6]$_8$ ([**10**][PF_6]$_8$).* Dark purple solid. Yield: 0.0985 g, 72.9%. IR (ATR): ν (cm^{-1}) 1588 (s, alkene, C=C), 1625 (s, pyridyl and imine, C=N). ^{1}H NMR ($(CD_3)_2CO$): δ (ppm) 1.06 and 1.11 (br m, 48H, $CH(CH_3)_{2\ p\text{-}cymene}$), 1.28 (br m, 4H, $NCH_2CH_{2\ core}$), 1.86−2.30 (overlapping m, 48H, $NCH_2CH_2CH_2N_{first\ branch}$, $NCH_2CH_2CH_2N_{second\ branch}$, $CH_{3\ p\text{-}cymene}$), 2.54−3.23 (overlapping m, 44H, $NCH_2CH_{2\ core}$, $NCH_2CH_2CH_2N_{first\ branch}$, $NCH_2CH_2CH_2N_{first\ branch}$, $NCH_2CH_2CH_2N_{second\ branch}$, $CH(CH_3)_{2\ p\text{-}cymene}$), 4.19 (br s, 40H, Cp-$CH_{unsubst\ ring}$), 4.43−4.71 (overlapping m, 48H, $NCH_2CH_2CH_2N_{second\ branch}$, 2 × Cp-CH), 5.90 and 6.21 (m, 32H, $Ar_{p\text{-}cymene}$), 6.98 and 7.55 (m, 16H, CH_{alkene}), 8.06 (m, 8H, Pyr), 8.34 (m, 8H, Pyr), 8.73 (br s, 8H, CH_{imine}), 9.50 (br s, 8H, Pyr). $^{13}C\{^1H\}$ NMR ($(CD_3)_2CO$): δ (ppm) 18.5, 21.4, 22.0 ($CH_{3\ p\text{-}cymene}$); 26.7, 50.8, 51.4, 51.7, 64.9 (CH_2); 68.1, 70.6 (Cp-CH); 69.5 (Cp-$CH_{unsubst.\ ring}$); 81.5 (C_{Cp}); 31.1, 84.3, 85.2, 85.3, 87.4 ($CH_{p\text{-}cymene}$); 103.9, 105.4 ($C_{p\text{-}cymene}$); 119.0, 137.1 (CH_{alkene}); 128.6, 133.4, 151.7 (CH_{Pyr}); 139.1, 151.7 (C_{Pyr}); 166.8 (CH_{imine}). Anal. Found for $C_{264}H_{312}N_{22}Cl_8F_{48}Fe_8P_8Ru_8$·9DCM (7256.558): C, 45.41; H, 4.11; N, 4.37. Calcd: C, 45.19; H, 4.58; N, 4.25. MS (HR-ESI-TOF, m/z): 667.4059 $[M]^{8+}$ (where M = [10][PF_6]$_8$ − 8PF_6). Mp: 203−204 °C.

Electrochemical Studies. Electrochemical studies were not performed on the ferrocenyl-derived precursors **1** and **2** and ligands **3**−**6**, **11**, and **12**, as the focus of this study was on the ferrocenyl-derived *p*-cymene-ruthenium complexes [7][PF_6]$_4$−[10][PF_6]$_8$, [13]-[PF_6], and [14][PF_6]. Cyclic voltammetric studies were performed at ambient temperature using a Bioanalytical Systems Inc. BAS 100W Electrochemical Analyzer with a one-compartment, three-electrode system comprising of a Pt-disk working electrode, a platinum-wire auxiliary electrode, and a Ag/Ag^+ reference electrode (0.01 M $AgNO_3$ and 0.1 M [*n*-Bu_4N][ClO_4] in anhydrous CH_3CN). The reported electrochemical potentials (given in Table 1) are with reference to this electrode. Measurements were made on anhydrous CH_3CN solutions, which were 2 mM in sample and contained 0.1 M [*n*-Bu_4N][ClO_4] as the background electrolyte. (***Caution!** Perchlorate salts of metal complexes are potentially explosive and the samples should be handled with care.*) Scan rates were optimized in an effort to obtain smoother voltammograms. Unless otherwise stated, the scan rate used was 100 mV s^{-1}. Under these conditions the ferrocene/ferrocenium couple, which was used as a reference, had $E_{1/2}$ = +0.12 V and ΔE_p = 0.10 V. All solutions were purged with argon, and voltammograms were recorded under a blanket of argon. The platinum working electrode was polished between runs.

X-ray Crystallography. Crystals of **1** and the heterometallic mononuclear complex [13][PF_6] were mounted on a STOE Image Plate Diffraction system equipped with a ϕ circle goniometer, using Mo Kα graphite monochromated radiation (λ 0.71073 Å) with ϕ

dx.doi.org/10.1021/om500809g | *Organometallics* 2014, 33, 5535−5545

range 0−200°. The structures were solved by direct methods using the program SHELXS-97, while the refinement and all further calculations were carried out using SHELXL-97.[45] The H atoms were included in calculated positions and treated as riding atoms using the SHELXL default parameters. The non-H atoms were refined anisotropically, using weighted least squares on F^2. Crystallographic details are summarized in Table S1 (Supporting Information). Figures 1 and 2 were drawn with ORTEP.[46]

Cell Proliferation Assay. Testing was done with cells growing in 96-well microtiter plates at 37 °C with 5% CO_2/air. Shortly before confluency, cells were trypsinized and a single-cell suspension was prepared. Cells were then plated out at a density of 250−2000 cells/well in 100 μL medium, depending on the cell line. Plates were returned to the incubator and cells allowed to attach and begin growing for 24 h before adding test substances. On the next day, one untreated plate for each cell line was removed, fixed with glutaraldehyde, and stored in the refrigerator; this plate served later as the control ($T_{c,0}$). All test substances were dissolved in DMF to a concentration of Fe of 5.0 mM, as calculated from the molecular formula. Next, these solutions were diluted 500-fold into culture medium to give twice the target concentration. Then, 100 μL of medium containing the test substance was added to each well, which already contained 100 μL of medium. The final solvent concentration (i.e., DMF) in each well was 0.1%. After 96 h incubation with substance, the culture medium was discarded and replaced with 100 μL/well of a 1% glutaraldehyde−buffer solution for 20 min to fix the cells. The fixing solution was discarded, and the cells were stored under 100 μL/well of PBS at 4 °C until staining. Before the cell mass was stained with crystal violet, the PBS medium was removed. Cell staining was done for 30 min with 100 μL/well of a 0.02% solution of crystal violet dissolved in PBS buffer solution. After the excess dye was discarded and the cells washed for 15 min in clear water, the cell-bound dye was redissolved in 100 μL/well 70% ethanol/water and the optical densities of the wells were measured at λ 570 nm with a microtiter plate reader. Cell proliferation (T/C_{corr}) was calculated by the equation

$$T/C_{corr}\ (\%) = \frac{\mathrm{O.D._T} - \mathrm{O.D._{c,0}}}{\mathrm{O.D._c} - \mathrm{O.D._{c,0}}} \times 100 \qquad (1)$$

where OD_T is the mean optical density of the treated cells, OD_c the mean optical density of the controls, and $OD_{c,0}$ the mean optical density at the time drug was added ($T_{c,0}$).

■ ASSOCIATED CONTENT

Supporting Information

Text, figures, a table, and CIF files giving details of syntheses and characterization data, NMR spectra, cyclic voltammograms, a plot of T/C_{corr}, and crystal data for **1** and [**13**][PF_6]·H_2O. This material is available free of charge via the Internet at http://pubs.acs.org. CCDC 1011457 (**1**) and 1011458 ([**13**][PF_6]·H_2O) also contain supplementary crystallographic data for this paper. These data can be obtained free of charge from The Cambridge Crystallographic Data Centre via www.ccdc.cam.ac.uk/data_request/cif.

■ AUTHOR INFORMATION

Corresponding Author

*G.S.S.: e-mail, gregory.smith@uct.ac.za; fax, +27-21-650 5195.

Notes

The authors declare no competing financial interest.

■ ACKNOWLEDGMENTS

Financial support from the University of Cape Town and the National Research Foundation (NRF) of South Africa and a generous donation of ruthenium trichloride trihydrate from the Anglo-American Platinum Limited Corporation/Johnson Matthey are gratefully acknowledged. We also thank members of COST Action CM1105 for useful discussions.

■ REFERENCES

(1) Gordon, M.; Hollander, S. *J. Med. Chem.* **1993**, *24*, 209−265.
(2) Wheate, N. J.; Walker, S.; Craig, G. E.; Oun, R. *Dalton Trans.* **2010**, *39*, 8097−8340.
(3) Pongratz, M.; Schluga, P.; Jakupec, M. A.; Arion, V. B.; Hartinger, C. G.; Allmaier, G.; Keppler, B. K. *J. Anal. At. Spectrom.* **2004**, *19*, 46−51.
(4) Bergamo, A.; Sava, G. *Dalton Trans.* **2007**, *13*, 1267−1272.
(5) (a) Dickson, N. R.; Jones, S. F.; Burris, H. A. *J. Clin. Oncol.* **2011**, *29*, (suppl.; abstract 2607). (b) Heffeter, P.; Atil, B.; Kryeziu, K.; Groza, D.; Koellensperger, G.; Korner, W.; Jungwirth, U.; Mohr, T.; Keppler, B. K.; Berger, W. *Eur. J. Cancer* **2013**, *49*, 3366−3375.
(6) Clarke, M. J.; Zhu, F. C.; Frasca, D. R. *Chem. Rev.* **1999**, *99*, 2511−2533.
(7) (a) Noffke, A. L.; Habtemariam, A.; Pizarro, A. M.; Sadler, P. J. *Chem. Commun.* **2012**, *48*, 5219−5246. (b) Süss-Fink, G. *Dalton Trans.* **2010**, *39*, 1673−1688. (c) Nazarov, A. A.; Hartinger, C. G.; Dyson, P. J. *J. Organomet. Chem.* **2014**, *751*, 251−260. (d) Bratsos, I.; Gianferrara, T.; Alessio, E.; Hartinger, C. G.; Jakupec, M. A.; Keppler, B. K., In *Bioinorganic Medicinal Chemistry*, Alessio, E., Ed.; Wiley-VCH: Weinheim, Germany, 2011; pp 151−174. (e) Liu, H.-K.; Sadler, P. J. *Acc. Chem. Res.* **2011**, *44*, 349−359. (f) Jakupec, M. A.; Galanski, M.; Arion, V. B.; Hartinger, C. G.; Keppler, B. K. *Dalton Trans.* **2008**, 183−194.
(8) (a) Casini, A.; Hartinger, C. G.; Nazarov, A. A.; Dyson, P. J. *Organometallic Antitumour Agents with Alternative Modes of Action*; Springer: Berlin, 2010; Top. Organomet. Chem. Vol. 32. (b) Ang, W. H.; Casini, A.; Sava, G.; Dyson, P. J. *J. Organomet. Chem.* **2011**, *696*, 989−998.
(9) Scolaro, C.; Bergamo, A.; Brescacin, L.; Delfino, R.; Cocchietto, M.; Laureneczy, G.; Geldbach, T. J.; Sava, G.; Dyson, P. J. *J. Med. Chem.* **2005**, *48*, 4161−4171.
(10) Chatterjee, S.; Kundu, S.; Bhattacharyya, A.; Hartinger, C. G.; Dyson, P. J. *J. Biol. Inorg. Chem.* **2008**, *13*, 1149−1155.
(11) Nowak-Sliwinska, P.; van Beijnum, J. R.; Casini, A.; Nazarov, A. A.; Wagnières, G.; van den Bergh, H.; Dyson, P. J.; Griffioen, A. W. *J. Med. Chem.* **2011**, *54*, 3895−3902.
(12) (a) Lease, N.; Vasilevski, V.; Carreira, M.; de Almeida, A.; Sanau, M.; Hirva, P.; Casini, A.; Contel, M. *J. Med. Chem.* **2013**, *56*, 5806−5818. (b) Donzello, M. P.; Viola, E.; Ercolani, C.; Fu, Z.; Futur, D.; Kadish, K. M. *Inorg. Chem.* **2012**, *51*, 12548−12559. (c) Gonzalez-Pantoja, J. F.; Stem, M.; Jarzecki, A. A.; Royo, E.; Robles-Escajeda, E.; Varela-Ramirez, A.; Aguilera, R. J.; Contel, M. *Inorg. Chem.* **2011**, *50*, 11099−11110. (d) Pelletier, F.; Comte, V.; Massard, A.; Wenzel, M.; Toulot, S.; Richard, P.; Picquet, M.; Le Gendre, P.; Zava, O.; Edafe, F.; Casini, A.; Dyson, P. J. *J. Med. Chem.* **2010**, *53*, 6923−6933. (e) Wenzel, M.; Bertrand, B.; Eymin, M. J.; Comte, V.; Harvey, J. A.; Richard, P.; Groessl, M.; Zava, O.; Amrouche, H.; Harvey, P. D.; Le Grande, P.; Picquet, M.; Casini, A. *Inorg. Chem.* **2011**, *50*, 9472−9480.
(13) Heinze, K.; Lang, H. *Organometallics* **2013**, *32*, 5623−5625.
(14) (a) van Staveren, D. R.; Metzler-Nolte, N. *Chem. Rev.* **2004**, *104*, 5931−5985. (b) Fouda, M. F. R.; Abd-Elzaher, M. M.; Abdelsamaia, R. A.; Labib, A. A. *Appl. Organomet. Chem.* **2006**, *21*, 613−625. (c) Braga, S. S.; Silva, A. M. S. *Organometallics* **2013**, *32*, 5626−5639.
(15) (a) Pigeon, P.; Top, S.; Vessières, A.; Huché, M.; Hillard, E. A.; Salmon, E.; Jaouen, G. *J. Med. Chem.* **2005**, *48*, 2814−2821. (b) Vessières, A.; Top, S.; Beck, W.; Hillard, E. A.; Jaouen, G. *Dalton Trans.* **2006**, *4*, 529−541.
(16) (a) Popova, L. V.; Babin, V. N.; Belousov, Y. A.; Nekrasov, Y. S.; Snegueva, A. E.; Borodina, N. P.; Shaposhnikova, G. M.; Bychenko, O. B.; Raevskii, P. M. *Appl. Organomet. Chem.* **1993**, *7*, 85−94. (b) Köpf-Maier, P.; Köpf, H.; Neuse, E. W. *J. Cancer Res. Clin.* **1984**, *108*, 336−340.
(17) (a) Nguyen, A.; Vessières, A.; Hillard, E. A.; Top, S.; Pigeon, P.; Jaouen, G. *Chimia* **2007**, *61*, 716−724. (b) Top, S.; Vessières, A.;

Cabestaing, C.; Laios, I.; Leclereq, G.; Provot, C.; Jaouen, G. *J. Organomet. Chem.* **2001**, *637*−*639*, 500−506.
(18) (a) Hillard, E. A.; Vessières, A.; Le Bideau, F.; Plazul, D.; Spera, D.; Huché, M.; Jaouen, G. *Chem. Med. Chem.* **2006**, *1*, 551−559 and references therein. (b) Wardman, P.; Candeias, L. P. *Radiat. Res.* **1996**, *145*, 523−531.
(19) Ornelas, C. *New J. Chem.* **2011**, *35*, 1973−1985.
(20) Goitia, H.; Nieto, Y.; Villacampa, D.; Kasper, C.; Laguna, A.; Gimeno, C. *Organometallics* **2013**, *32*, 6069−6078.
(21) Rajput, J.; Moss, J. R.; Hutton, A. T.; Hendricks, D. T.; Arendse, C. E.; Imrie, C. *J. Organomet. Chem.* **2004**, *689*, 1553−1568.
(22) (a) Tauchman, J.; Süss-Fink, G.; Štěpnička, P.; Zava, O.; Dyson, P. J. *J. Organomet. Chem.* **2013**, *723*, 233−238. (b) Auzias, M.; Gueniat, J.; Therrien, B.; Süss-Fink, G.; Renfrew, A. K.; Dyson, P. J. *J. Organomet. Chem.* **2009**, *694*, 855−861. (c) Auzias, M.; Therrien, B.; Süss-Fink, G.; Štěpnička, P.; Ang, W. H.; Dyson, P. J. *Inorg. Chem.* **2008**, *47*, 578−583.
(23) Billecke, C.; Finniss, S.; Tahash, L.; Miller, C.; Mikkelsen, T.; Farrell, N. P.; Bogler, O. *Neuro-Oncology* **2006**, *8*, 215−226.
(24) (a) Astruc, D.; Boisselier, E.; Ornelas, C. *Chem. Rev.* **2010**, *110*, 1857−1959. (b) Newkome, G. R.; Shreiner, C. *Chem. Rev.* **2010**, *110*, 6338−6442. (c) Newkome, G. R.; He, E.; Moorefield, C. N. *Chem. Rev.* **1999**, *99*, 1689−1746. (d) Seek-Ho, H.; Shreiner, C. D.; Moorefield, C. N.; Newkome, G. R. *New J. Chem.* **2007**, *31*, 1192−1217. (e) Angurell, I.; Rossell, O.; Seco, M. *Inorg. Chim. Acta* **2014**, *409*, 2−11.
(25) (a) Govender, P.; Therrien, B.; Smith, G. S. *Eur. J. Inorg. Chem.* **2012**, 2853−2862. (b) El Kazzouli, S.; El Brahmi, N.; Mignani, S.; Bousmina, M.; Zablocka, M.; Majoral, J.-P. *Curr. Med. Chem.* **2012**, *19*, 4995−5010.
(26) (a) Govender, P.; Antonels, N. C.; Mattsson, J.; Renfrew, A. K.; Dyson, P. J.; Moss, J. R.; Therrien, B.; Smith, G. S. *J. Organomet. Chem.* **2009**, *694*, 3470−3476. (b) Govender, P.; Renfrew, A. K.; Clavel, C. M.; Dyson, P. J.; Therrien, B.; Smith, G. S. *Dalton Trans.* **2011**, *40*, 1158−1167. (c) Govender, P.; Sudding, L. C.; Clavel, C. M.; Dyson, P. J.; Therrien, B.; Smith, G. S. *Dalton Trans.* **2013**, *42*, 1267−1277.
(27) Govender, P.; Edafe, F.; Makhubela, B. C. E.; Dyson, P. J.; Therrien, B.; Smith, G. S. *Inorg. Chim. Acta* **2014**, *409*, 112−120.
(28) Payne, R.; Govender, P.; Therrien, B.; Clavel, C. M.; Dyson, P. J.; Smith, G. S. *J. Organomet. Chem.* **2013**, *729*, 20−27.
(29) (a) Liu, W.-Y.; Xu, Q.-H.; Ma, Y.-X.; Liang, Y.-M.; Dong, N.-L.; Guan, D.-P. *J. Organomet. Chem.* **2001**, *625*, 128−131. (b) Gallei, M.; Klein, R.; Rehahn, M. *Macromolecules* **2010**, *43*, 1844−1854.
(30) Reyes, M. I.; Vazquez Garcia, R. A.; Klimova, T.; Klimova, E.; Ortiz-Frade, L.; Martinez Garcia, M. *Inorg. Chim. Acta* **2008**, *361*, 1597−1605.
(31) Williams, D. H.; Fleming, I. In *Spectroscopic Methods in Organic Chemistry*; McGraw-Hill: United Kingdom, 1989; Table 3.27.
(32) Yang, Y.-F.; Chen, Y.; Xie, T.; Liang, Y.-M. *Synth. Commun.* **2002**, *32*, 2627−2631.
(33) Jansen, J. F. G. A.; de Brabander-van den Berg, E. M. E.; Meijer, E. W. *Science* **1994**, *266*, 1226−1269.
(34) (a) Smolenski, P.; Pruchnik, F. P.; Ciunik, Z.; Lis, T. *Inorg. Chem.* **2003**, *42*, 3318−3322. (b) Pruchnik, F. P.; Smolenski, P.; Galdecka, E.; Galdecki, Z. *New J. Chem.* **1998**, *22*, 1395−1398.
(35) (a) Renfrew, A. K.; Phillips, A. D.; Tapavicza, E.; Scopelliti, R.; Rothlisberger, U.; Dyson, P. J. *Organometallics* **2009**, *28*, 5061−5071. (b) Ang, W. H.; Daldini, E.; Scolaro, C.; Scopelliti, R.; Juillerat-Jeanneret, L.; Dyson, P. J. *Inorg. Chem.* **2006**, *45*, 9006−9013.
(36) (a) Chavian, N.; Vezin, H.; Dive, D.; Touati, N.; Paul, J. F.; Buisine, E.; Biot, C. *Mol. Pharmaceutics* **2008**, *5*, 710−716. (b) Dubar, F.; Bohic, S.; Slomianny, C.; Morin, J. C.; Thomas, P.; Kalamou, H.; Guerardel, Y.; Cloetens, P.; Khalife, J.; Biot, C. *Chem. Commun.* **2012**, *48*, 910−912. (c) Biot, C.; Castro, W.; Botte, C. Y.; Navarro, M. *Dalton Trans.* **2012**, *41*, 6335−6349.
(37) Matsinha, L. C.; Malatji, P.; Hutton, A. T.; Venter, G. A.; Mapolie, S. F.; Smith, G. S. *Eur. J. Inorg. Chem.* **2013**, 4318−4326.
(38) (a) Tauchman, J.; Therrien, B.; Süss-Fink, G.; Štěpnička, P. *Organometallics* **2012**, *31*, 3985−3994. (b) Mai, J.-F.; Yamamoto, Y. *J. Organomet. Chem.* **1998**, *560*, 223−232.
(39) (a) Štěpnička, P.; Gyepes, R. *Organometallics* **1997**, *16*, 5089−5095. (b) Sixt, T.; Sieger, M.; Krafft, M. J.; Bubrin, D.; Fiedler, J.; Kaim, W. *Organometallics* **2010**, *29*, 5511−5516. (c) Therrien, B.; Vieille-Petit, L.; Jeanneret-Gris, J.; Štěpnička, P.; Süss-Fink, G. *J. Organomet. Chem.* **2004**, *689*, 2456−2463.
(40) Lopez, C.; Bosque, R.; Perez, S.; Roig, A.; Molins, E.; Solans, X.; Font-Bardia, M. *J. Organomet. Chem.* **2006**, *691*, 475−484.
(41) Bracht, K.; Boubakari; Gruner, R.; Bednarski, P. J. *Anticancer Drugs* **2006**, *17*, 41−51.
(42) Hillard, E. A.; Pigeon, P.; Vessières, A.; Amatore, C.; Jaouen, G. *Dalton Trans.* **2007**, 5073−5081.
(43) (a) Bennett, M. A.; Smith, A. K. *J. Chem. Soc., Dalton Trans.* **1974**, *2*, 233−241. (b) Sonoda, A.; Moritani, I.; Saraie, T.; Wada, T. *Tetrahedron Lett.* **1969**, 2943−2946.
(44) Fulmer, G. R.; Miller, A. J. M.; Sherden, N. H.; Gottlieb, H. E.; Nudelman, A.; Stoltz, B. M.; Bercaw, J. E.; Goldberg, K. I. *Organometallics* **2010**, *29*, 2176−2179.
(45) Sheldrick, G. M. *Acta Crystallogr., Sect. A* **2008**, *A64*, 112−122.
(46) Farrugia, L. *J. Appl. Crystallogr.* **1997**, *30*, 565.